JOURNAL OF MATERIALS RESEARCH AND TECHNOLOGY 2023;24:3717–3730

Available online at www.sciencedirect.com

jmr&t Journal of Materials Research and Technology

journal homepage: www.elsevier.com/locate/jmrt

Original Article

Evaluation of photothermal conversion performance of shape-stabilized phase change materials using a heat flux evolution curve

Safna Nishad [a], *Himyan Mohammed* [a], *Patrik Sobolciak* [a], *Igor Krupa* [a,b,*]

[a] *Center for Advanced Materials, Qatar University, 2713, Doha, Qatar*

[b] *Materials Science and Technology Graduate Program, College of Arts and Sciences, Qatar University, 2713, Doha, Qatar*

ARTICLE INFO

Article history:
Received 25 December 2022
Accepted 6 April 2023
Available online 12 April 2023

Keywords:
Photothermal conversion
Thermal energy storage
Heat flux evolution curve
Polymer-based phase change material
The conversion efficiency

ABSTRACT

Phase change materials are promising alternatives for solar energy harvesting by photothermal conversion and thermal energy storage. In this work, a shape-stabilized phase change material (PCM) was prepared by hot-melt blending of paraffin wax (PW), high-density polyethylene (HDPE), and expanded graphite (EG) to investigate the photothermal conversion and storage performance using a heat flux evolution curve. This study introduced the heat flux evolution curve for the first time to accurately measure phase change duration, which is otherwise underestimated by the conventional temperature curves. The impact of various component compositions on thermal conductivity, energy storage density, PCM leakage, and photothermal conversion efficiency was evaluated experimentally. The results showed that the addition of 20 wt% EG enhanced the thermal conductivity of the composite by 305%. The total energy storage density of the composite varied in the range of 116.7–138.5 J/g during the photothermal conversion study. The composite with 15 wt% EG and 50 wt% PW exhibited a photothermal conversion efficiency of 79.8% when calculated from the temperature evolution curve and 61.8% from the heat flux evolution curve. This difference in efficiency indicates that the temperature evolution curve accounts only for the phase change of PCMs at the point of temperature measurement, while the heat flux evolution curve estimates the phase change of whole PCMs in the composite. Therefore, this work not only provides a shape-stabilized phase change material for the effective utilization of solar energy but also provides some guidelines to accurately calculate the photothermal conversion efficiency.

* Corresponding author.
E-mail address: igor.krupa@qu.edu.qa (I. Krupa).

https://doi.org/10.1016/j.jmrt.2023.04.047

1. Introduction

In recent years, the global energy demand has increased with the rapid social and economic development of society. The overexploitation of conventional energy resources leads to environmental concerns and the depletion of fossil fuels. Therefore, the development of efficient and renewable energy resources is necessary for the sustainable growth of humanity. Solar energy is an important renewable energy source due to its endless reserves [1,2]. Studies on the efficient utilization of solar energy have gained much attention due to its carbon-neutral and renewable characteristics. Solar energy is often converted to electrical and thermal energy by photovoltaic and photothermal conversion techniques [3,4]. Photothermal conversion is the most efficient and simple solar energy utilization technique for space and water heating [5–7], power generation [8], desalination [9], etc. However, the unstable and intermittent properties of solar energy require thermal energy storage (TES) systems to meet the continuous energy demand. Phase change materials (PCMs) are widely adopted for TES systems due to their high energy storage density and isothermal behavior [10]. Among various organic and inorganic PCMs, paraffin waxes are usually used in practical applications due to the commercial availability of various grades having different phase change temperatures and latent heat, non-corrosiveness, negligible supercooling, and phase segregation compared to inorganic salt hydrates [11]. However, low thermal conductivity, poor photoabsorption and low mechanical strength are the limiting factors of paraffins in practical applications of energy conversion and storage [12].

There are different strategies adopted to overcome the above limitations, including microencapsulation in the polymeric matrix [13–15], PCMs impregnated in porous materials [16–18], and blending with polymers [19–23]. Recently, polymeric phase change composites have attracted the attention of researchers due to their (i) cost-effectiveness, (ii) high mechanical strength, (iii) efficiency in leakage prevention and heat storage capacity enhancement, (iv) flexibility, (v) nontoxic, nonflammable and noncorrosive nature, (vi) lightweight characteristics with a high strength/weight ratio, and (vii) abundance and availability.

Among various polymeric phase change composites, polyethylene and paraffin wax blends have attracted much attention due to their chemical and structural similarities [19,24]. They provide good processability, are lightweight and are low-cost. Krupa et al. [24] investigated the energy storage properties of low-density polyethylene blends (LDPE) with paraffin wax. The LDPE matrix kept the composite in a compact shape, while the paraffin wax stored a large amount of latent heat during melting. Furthermore, blends of high-density polyethylene (HDPE) and paraffin wax were reported to have excellent shape stability and heat storage capacity [25–27]. Adding a small fraction of expanded graphite into the polymer phase change composite not only increases the thermal conductivity but also enhances the photoabsorption capacity [28]. Although the addition of nanomaterials including graphene [29–31], CNTs [32,33] and MoS_2 [34,35] have been widely reported in the literature, the smaller size and large surface area of those fillers require additional treatment for efficient dispersion in polymeric matrices. Therefore, expanded graphite serves better for polymeric phase change composites due to its constant properties, availability in various sizes and low price in addition to its easy dispersion [36–38]. Previous studies reported photothermal conversion performances of phase change composites with expanded graphite and different polymers such as thermoplastic elastomer [37], ethylene-propylene-diene [39], polyoxyethylene [36] etc. Considering the availability and recyclability of polyethylene, phase change composites based on polyethylene with better photothermal conversion performances would break through into sustainable harvesting of solar energy.

In addition, the determination of the thermal properties and photothermal conversion performance of the composites at physically representative sizes is important to evaluate the efficiency in practical applications. Previous studies used differential scanning calorimetry (DSC) to estimate the thermal properties of the composites (i.e., latent heat and specific heat capacities). However, the measured thermal properties by DSC are significantly influenced by the sample mass, heterogeneity, and scanning rate [40,41]. Recently, the thermal characterization of composites with representative sizes was evaluated using a new device based on the transient guarded hot plate technique (TGHPT) [42]. Various thermal properties of PCMs, including latent heat, sensible heat, specific heat capacities, thermal conductivities, thermal storage, and release of resin epoxy/PW [43,44], LDPE/PW [45], LLDPE/PW/EG Ref. [28] composites at variable component mass fractions, were determined using the newly constructed device. The thermophysical properties of the composite obtained from this method are more representative of practical applications due to the utilization of large-sized samples.

Moreover, previous studies measured the phase change duration of the composite (during photothermal conversion study) between the start and endpoints of the temperature plateau in the temperature evolution curves obtained either on the top surface or the middle of the specimen [30,32,46–49]. The temperature evolution curve only shows the phase change of the PCM at the measurement location. It may not reflect the phase change process in the whole specimen and therefore overestimate the conversion efficiency. This is due to the underlying assumption in the efficiency calculation that all PCMs undergo phase change during the conversion study.

Therefore, in this study, the heat flux evolution curves are introduced for the first time to accurately estimate the phase change duration. The method estimates the time required for the completion of the phase change in the whole composite specimen during solar irradiation, thereby satisfying the assumption in the conversion efficiency calculation. The thermal properties of the HDPE/PW/EG composites are measured from the TGHPT method on physically representative sample size and are used to estimate the photothermal conversion efficiencies of the composites. With the increase in EG and PW mass fraction, the enhancement in the thermal conductivity and photothermal conversion efficiency was investigated.

2. Experimental

2.1. Materials

High-density polyethylene (QChem, Qatar), paraffin wax RT42 (Rubitherm® Technologies GmbH, Germany), and expanded graphite with an average particle size (D50) of 200 μm (SGL Carbon's SIGRATHERM®, Germany) were used for the preparation of the phase change composite.

2.2. Preparation of the composite

The PCM blends were prepared by mixing all components in a 50 mL mixing chamber of a Brabender® Plastograph® EC W50 PLE 331 (Duisburg, Germany) for 10 min at 160 °C and a mixing speed of 35 rpm.

The samples of cylindrical shape were prepared from mixtures using a hydraulic mounting press machine (Carver 3895, USA) by hot-pressing at 160 °C for 3 min.

Table 1 summarizes the composition, size, and density of the different samples used in this study.

2.3. Material characterization

For thermal conductivity and diffusivity measurements, specimens with a diameter of 7 cm and thickness of 9 mm were compression molded in the hydraulic mounting press. The thermal conductivity and thermal diffusivity were measured using a multipurpose apparatus (ISOMET, Applied Precision, Slovakia). The thermal response of the composite was measured as a function of time to the heat flow impulses generated by the electrical heating of the resistor heater. All the samples were tested three times at room temperature using a flat probe. The method yields reproducible thermal conductivity with an accuracy of 5% of reading+0.001 W/m.°C.

The leakage experiment was conducted to investigate the mass loss of PW from the HDPE/PW/EG composites when placed in an oven at a temperature over the melting point. The strips of HDPE/PW/EG specimens with dimensions of 60 × 60 × 1mm were placed in an oven at 60 °C for 12 days. The samples were weighed daily using an analytical balance after cleaning them from excessive and melted PW on the top surfaces using a clean cloth. The percentages of the PW mass loss in the composite were calculated according to the equation:

Table 1 – Composition of the prepared samples, their sizes, and densities.

Samples	HDPE/PW/EG w/w/w	Thickness mm	Diameter mm	Density g/cm^3
S1	50/50/0	8.49	67.53	0.921
S2	55/40/5	8.79	67.07	0.941
S3	50/40/10	9.30	67.60	0.982
S4	45/40/15	8.78	67.56	0.989
S5	40/40/20	9.09	67.78	1.004
S6	45/50/5	8.65	67.36	0.945
S7	40/50/10	8.25	67.50	0.971
S8	35/50/15	8.61	68.06	0.990

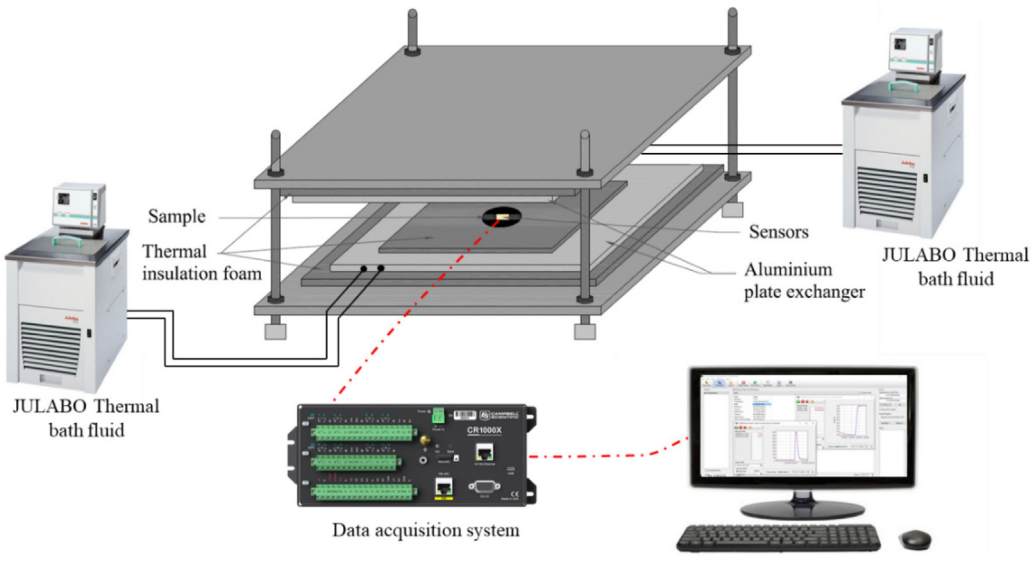

Fig. 1 – Transient guarded hot plate technique.

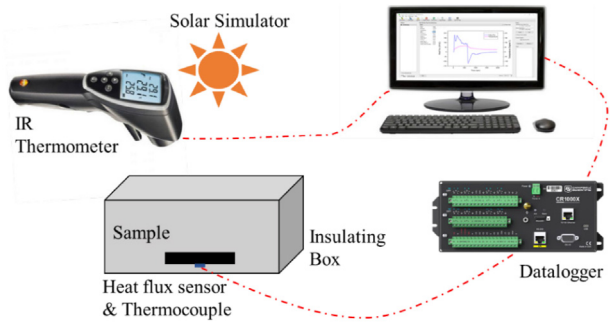

Fig. 2 – A schematic of the photothermal energy conversion and storage performance measuring system.

Table 2 – Thermal conductivities and diffusivities of composites.

Samples	λ_{eff} (SD) W/m.°C	α (SD) mm^2/s	I $_{\lambda eff}$%
S1	0.379 (0.003)	0.238 (0.003)	90
S2	0.447 (0.001)	0.269 (0.001)	125
S3	0.609 (0.001)	0.348 (0.001)	205
S4	0.639 (0.001)	0.354 (0.001)	220
S5	0.806 (0.001)	0.435 (0.002)	305
S6	0.519 (0.003)	0.306 (0.003)	160
S7	0.561 (0.001)	0.329 (0.001)	180
S8	0.707 (0.001)	0.368 (0.001)	255

$$Mass\ loss = \frac{(m_0 - m)}{m_0 \times w} \times 100\ (\%) \quad (1)$$

where m_0 is the initial mass of the specimen, m is the actual mass of the specimen and w is the mass fraction of paraffin wax.

The changes in the microstructure of PCMs were investigated as two-dimensional (2D) images by scanning electron microscopy (SEM, FEI Quanta 200 ESEM, Thermo Fisher Scientific™, USA) at high magnification and spatial resolution to achieve high-quality images. The working distance (WD) between the source of electrons and the exposed surface of the sample did not exceed 9.0 mm. The SEM system was operated with a moderate acceleration voltage equal to 5.0 kV. Furthermore, the tested specimens were coated by a thin layer of gold (Au) with a thickness of a few angstroms to ensure a higher resolution of captured images, as well as to prevent charging of the surface and to promote the emission of secondary electrons.

The latent heat of phase change was measured using differential scanning calorimetry (DSC 8500, Perkin Elmer, USA) at a rate of 10 °C/min to compare the values obtained from the transient guarded hot plate technique. The composite sample of mass ranging between 3 and 15 mg was taken. All measurements were repeated three times, and average values of latent heat at the second heating cycle are presented with an accuracy of ±0.05 °C for the temperature and 0.2% for the heat flow.

2.4. *Thermal characterization using the transient guarded hot plate technique*

The thermal properties of the composites were determined by the TGHPT, as shown in Fig. 1. A cylindrical sample (for size, see Table 1) was placed between two isothermal aluminum plate-type heat exchangers connected to thermoregulated fluid baths that allowed fine regulation of temperature with a precision of 0.1 °C. Heat flux sensors and T-type thermocouples were located on both sides of the samples to measure the evolution of heat flux and temperature on each face of the composite. The lateral sides of the composite and the plate exchangers were insulated with polyurethane foam. The sensors were connected to a CR1000X datalogger (CampBell Scientific, USA) to measure the temperature and heat flux exchanged during the phase change process. Experimental data were recorded at regular time steps of 5 s.

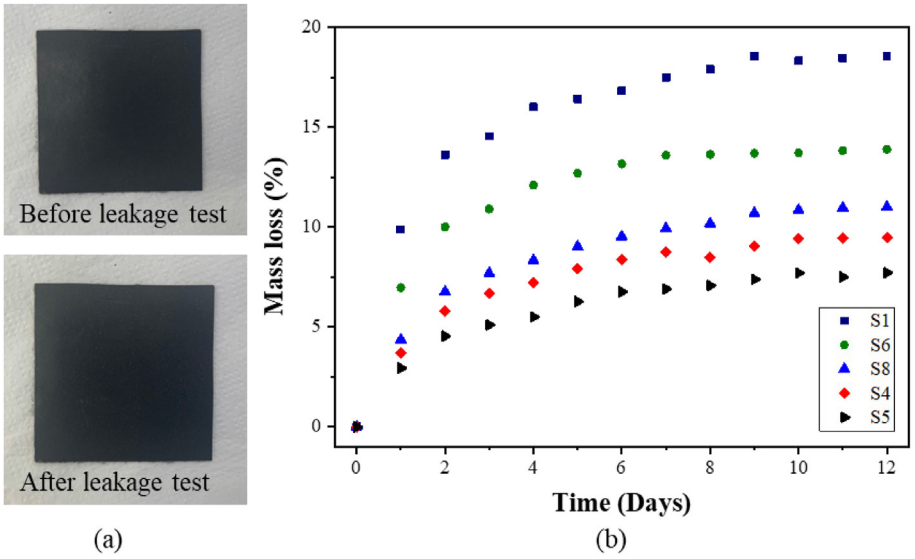

Fig. 3 – (a) Images of S8 composite before and after leakage test and (b) PW mass loss (%) in the composites during 12 days of leakage test.

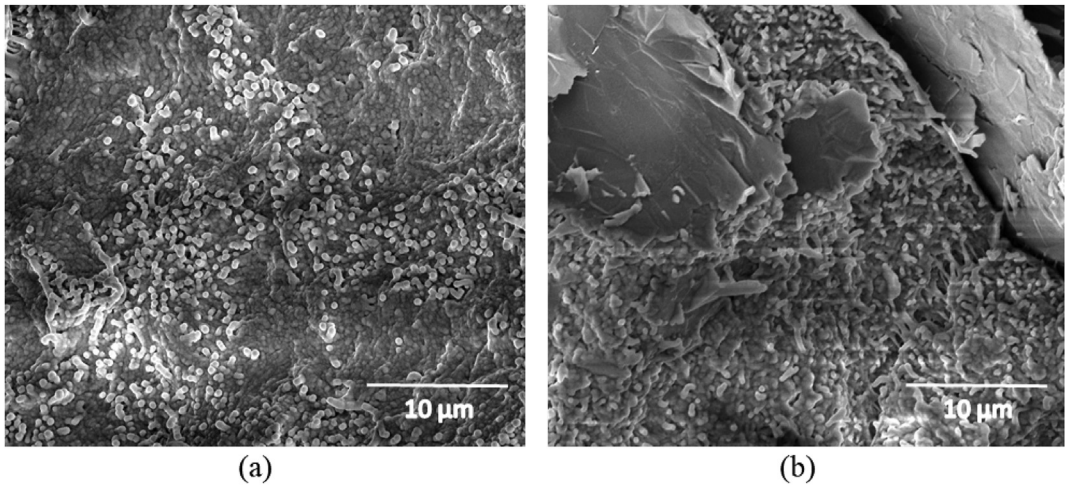

Fig. 4 – SEM images of a) S1 and b) S8.

2.5. *Photothermal conversion testing*

The light to thermal conversion and storage test was conducted under simulated sunlight using a solar simulator (Sunlite, ABET Technologies). The cylindrical sample was placed inside a foam box, and the solar simulator was irradiated under a constant intensity of 1000 W/m^2. The variations in the sample top and bottom temperature and heat flux during the energy conversion and storage process were obtained using an infrared thermometer (Testo 845, Germany), a T-type thermocouple, and a heat flux sensor (Captec, France), respectively. The data collection and analysis were carried out using a CR1000X datalogger (CampBell Scientific, USA). A schematic of the photo of the thermal conversion test system is shown in Fig. 2.

3. Results and discussion

3.1. *Thermal conductivity and diffusivity*

Table 2 summarizes the measured thermal conductivities (λ_{eff}), diffusivities (α), and associated standard deviations of the composites. The addition of 50 wt% PW into sample S1 reduced the thermal conductivity from 0.46 W/m.°C (neat HDPE) to 0.38 W/m.°C due to the lower thermal conductivity of PW (0.20 W/m.°C). The addition of EG into the composite significantly enhanced the thermal conductivity and diffusivity of the composite. The thermal conductivity increased with the EG mass fraction, as shown in Table 2.

The intensification of thermal conductivity with the addition of EG was calculated by the equation:

$$I_{\lambda\ eff} = \left(\lambda_{eff} - \lambda_{PW}\right)/\lambda_{PW} \times 100 \quad (2)$$

where λ_{eff} is the effective thermal conductivity of the composite and λ_{PW} is the thermal conductivity of pure PW (i.e., 0.20 W/m.°C). The intensification factor of the composites with 50 wt% PW increased from 90% to 255% with increasing EG loading (0–15 wt%). Moreover, the thermal conductivity was enhanced by approximately 305% for the composite with 20 wt% EG and 40 wt% PW.

3.2. *The shape stability*

The shape stability of the composites was investigated by the leakage test as described in section 2.3. Fig. 3 shows the mass loss of S1, S4, S5, S6, and S8 over the period of 12 days and the

Table 3 – Specific heat capacities of composites in solid and liquid states at different temperature ranges determined from TGHPT.

Sample	Solid Specific heat capacity, C_{ps} (J/g.°C)				Liquid Specific heat capacity, C_{ps} (J/g.°C)			
	20–25 °C	25–30 °C	30–35 °C	Average (20–35 °C)	45–50 °C	50–55 °C	55–60 °C	Average (45–60 °C)
S1	2.72	2.97	3.74	3.14	2.63	2.55	2.54	2.57
S2	2.70	3.04	3.13	2.96	2.67	2.56	2.57	2.60
S3	2.74	2.97	3.01	2.90	2.40	2.31	2.33	2.34
S4	2.30	2.53	2.76	2.53	2.22	2.15	2.16	2.18
S5	2.21	2.42	2.62	2.42	2.18	2.12	2.15	2.15
S6	2.45	2.71	2.84	2.67	2.03	2.18	2.21	2.14
S7	2.44	2.70	2.67	2.60	2.04	2.16	2.16	2.12
S8	2.33	2.57	2.52	2.47	1.83	1.99	2.00	1.94

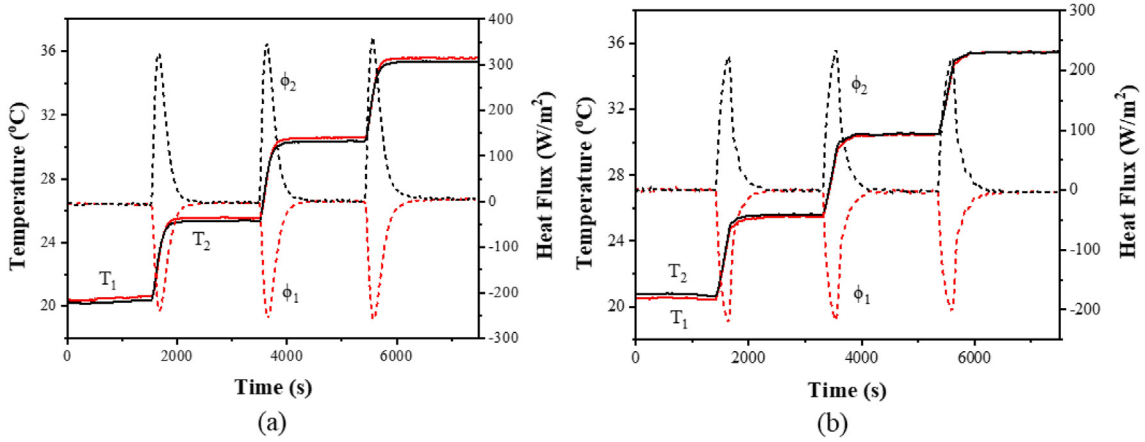

Fig. 5 – Heat flux and temperature evolution of composites in the solid state (from 20 to 35 °C): (a) S5 and (b) S8.

images of the S8 composite before and after the leakage test. The images of the composite S8 in Fig. 3a indicate its shape stability due to the presence of a polymeric matrix in the composite. As observed in Fig. 3b, the addition of EG (0–20%) decreased the PW leakage from 20% to 7%. This improvement can be due to the action of EG as a porous structure where the capillary and surface tension forces prevent PW leakage [20]. Moreover, at the same EG fraction, an increase in the PW content increased the PW leakage due to the lack of a polymer supporting matrix. However, the reduction in PW will decrease the thermal storage capacity. Therefore, care must be taken while choosing the optimum proportion of the components.

3.3. *Microstructure of the composite*

SEM images of composites S1 and S8 are shown in Fig. 4. The white droplets indicate PW. The images clearly distinguish HDPE from PW, indicating the immiscibility of the components, which is necessary to have well-distinguished melting points for HDPE and PW (Fig. 4a). EG particles in the S3 composite are recognized by the graphite sheets in Fig. 4b. During composite preparation, the melted HDPE and PW are penetrated between graphite sheets of EG.

3.4. *The heat capacity in liquid and solid states*

To determine the sensible heat and specific heat capacity of the composite, the samples were heated in the solid state or liquid state, and the evolutions of temperatures (T_1 and T_2) and heat fluxes (φ_1 and φ_2) were measured on each side of the composite. The tests were conducted under the dynamic temperature conditions recommended by the ASTM C518 standard [50].

Initially, the two heat exchanger plates were maintained at an isothermal state, T_{ini}. The composite was then evolved to a final isothermal temperature, T_{end}, by gradual heating of the plate exchanger. During this change in temperature, the composite stores sensible heat Q_{sens} due to the internal variation in the system energy. The specific heat capacity can be calculated from the integral of the heat flux during the temperature change (t_{ini} to t_{end}). The stored sensible heat is given by Eq. (3).

$$Q_{sens} = \frac{1}{\rho.e}\int_{t_{ini}}^{t_{end}} (\Delta\varphi - \Delta\varphi_{loss}).dt = C_p.(T_{end} - T_{ini}) \quad (3)$$

where C_p is the specific heat capacity, $\Delta\varphi$ is the difference in the measured heat flux at each time step during the time, dt, $\Delta\varphi_{loss}$ is the heat flux lost from the heat exchanger by the flux

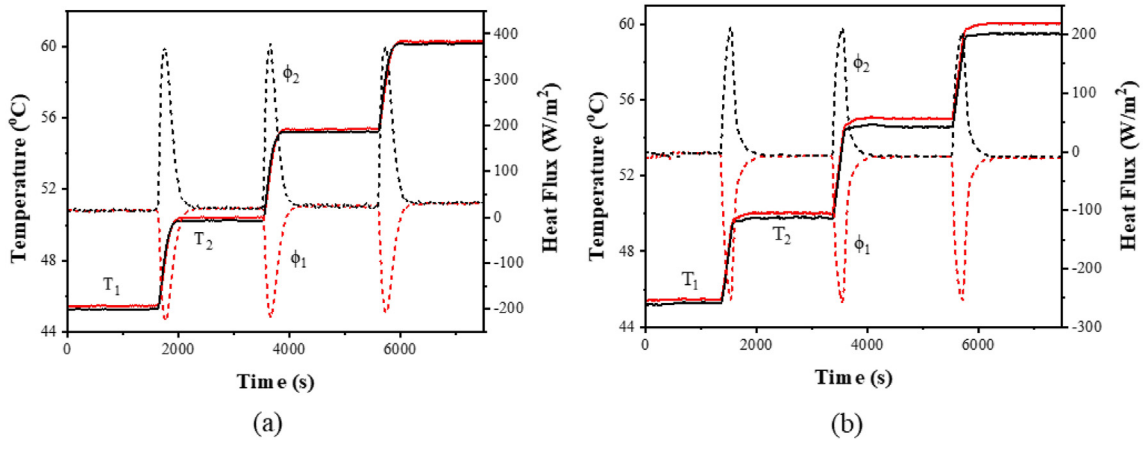

Fig. 6 – Heat flux and temperature evolution of composites in the liquid state (from 45 to 60 °C): (a) S1 and (b) S2.

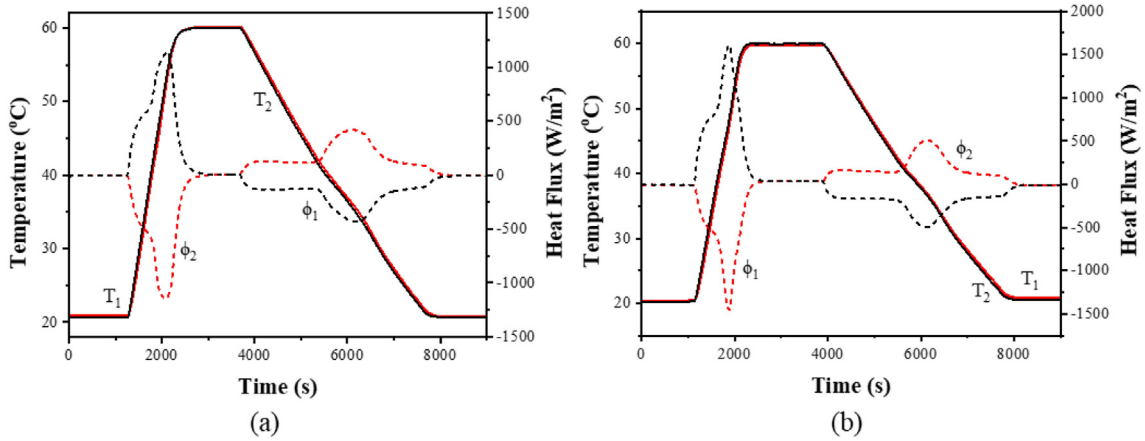

Fig. 7 – Heat flux and temperature evolution from solid to liquid for (a) S1 and (b) S5.

sensors and to the surroundings, e is the thickness of the composite, and ρ is the density of the composite.

To determine the heat loss, a calibration test was conducted by operating the device without the test specimen [51]. The heat flux evolution curves indicate the loss of heat from the heat exchanger through the flux sensors and to the surroundings. This calibration is crucial for accurate specific heat capacity determination, which is otherwise overestimated in some previous studies [20,28]. The calibration test was conducted at the same temperature range as those used for specific heat capacity determination because it varies with the temperature. The details of calibration test are given in the Supplementary Material.

To determine the apparent specific heat capacities of the composite in the solid and liquid states, different temperature intervals (20–25 °C, 25–30 °C and 30–35 °C for the solid state and 45–50 °C, 50–55 °C and 55–60 °C for the liquid state) were tested. The specific heat capacities of various composites are shown in Table 3. The sensible heat storage in the composites for solid and liquid states are shown in Figs. 6 and 7 for S1, S2, S5 and S8. Fig. 5 presents the variation in the heat flux and temperature of the composites in the solid phase for three temperature ranges (i.e., 20–25 °C, 25–30 °C, and 30–35 °C), while Fig. 6 presents similar results for the liquid phase at three temperature ranges (i.e., 45–50 °C, 50–55 °C, and 55–60 °C). The temperature measurements on the top and bottom surfaces of the sample evolve asymptotically to the set point. The heat flux increases quickly at the beginning and then goes to zero when the composite reaches a new state of balance at the end of the test. The C_p values were calculated using Eq. (3). A slight increase in C_p for the solid phase and a slight decrease in C_p for the liquid phases were noticed with the increase in temperature, as shown in Table 3. Moreover, C_p values slightly decrease with an increase in EG content due to the lower specific heat capacity of EG, which was 0.75 kJ/kg.°C.

The average C_p values at three temperature ranges for each composite were used to calculate the apparent latent heat, as discussed in the next section.

3.5. *Energy storage and release*

To determine the total energy storage and release, the temperature was varied from 20 °C to 60 °C. Initially, the sample was placed at an isothermal temperature (T_{ini} = 20 °C). Subsequently, the sample was heated to 60 °C by modifying the temperature set point of the thermoregulated bath. Between these steady states, the composite stores energy as sensible and latent heat. Finally, the sample was cooled to T_{ini} = 20 °C. Fig. 7 presents the heat flux and temperature evolutions of the composites showing the thermal energy storage and release.

The total energy for a temperature variation from 20 °C to 60 °C includes the sensible and latent heat. The latent heat can be calculated by subtracting the sensible heat from the total energy. The total energy absorbed and released by the

Table 4 – Total heat, sensible heat in the solid and liquid state of PW, and latent heat of various composites.

Sample	Q_{total} (J/g)	Average Q_{sens} (J/g)		Latent Heat (L_m)		
		Solid	Liquid	TGHPT J/g	DSC J/g	Error%
S1	177.3	69.1	46.2	62.0 (1.2)	60.8 (3.6)	2
S2	154.5	65.1	46.8	42.6 (1.1)	45.0 (5.2)	6
S3	150.8	63.8	42.3	44.7 (1.3)	46.1 (4.3)	3
S4	135.7	55.6	39.2	40.9 (2.1)	42.5 (4.4)	4
S5	139.6	53.2	38.7	47.7 (1.1)	44.0 (3.8)	8
S6	158.0	58.7	38.5	60.8 (2.1)	60.7 (4.1)	0
S7	157.9	57.3	38.2	62.4 (1.9)	63.1 (5.1)	1
S8	153.5	54.5	34.9	64.1 (1.5)	63.6 (4.4)	1

composite during the isothermal process can be calculated by Eq. (4).

$$Q_{total} = Q_{sens} + L_m = \frac{1}{\rho.e}\int_{t_{ini}}^{t_{end}} (\Delta\varphi - \Delta\varphi_{loss}).dt$$

$$= \left(C_p(solid).\Delta T(solid) + C_p(liquid).\Delta T(liquid)\right) + L_m \left(\frac{J}{g}\right) \quad (4)$$

where C_p(solid) and C_p(liquid) are the average solid-state and the liquid state C_p of the material, ΔT(solid) and ΔT(liquid) are the temperature variations for the material in the solid and liquid states, and L_m is the latent heat of melting.

Table 4 summarizes the values of the total heat calculated as the average values of the second heating and cooling cycles of the samples, sensible heat in the solid and liquid states of PW, and L_m of the composites during the temperature evolution of approximately 20–60 °C. Sensible heat is calculated according to Eq. (3). Using the average C_p values (listed in Table 3) in the solid state and liquid state for exact experimental temperatures. The total heat and apparent latent heat are calculated according to Eq. (4).

Uncertainty analysis has been conducted to estimate the measurement uncertainty arise from the temperature, heat flux, thickness and mass estimations and is given in the Supplementary material. The results show that the uncertainties in specific heat capacity and latent heat are 5.1 and 6%, respectively. However, the measurements were conducted three times on each composite and the standard deviation in the latent heat is given in Table 4. The uncertainty calculated from the replicates varied between 1.1% and 3%, which remain quite acceptable and allows validating the results proposed in this study.

The latent heat of melting of the composites was also investigated by DSC and compared with that measured by TGHPT in Table 4. The larger standard deviations in the DSC measurements indicate their dependence on the sample mass, geometry, and homogeneity of the composite [40,41,52]. For example, apart from the tiny portion of the composite tested in DSC, the homogeneity of the composite is questionable considering the immiscibility of the components in the composite. Therefore, the larger samples of the composites tested using TGHPT will provide more representative results with negligible variance. However, it is worth noting that the error in the measured latent heat by the two methods varied between 0% and 8% (Table 4), indicating the suitability of the TGHPT method for predicting the thermal properties of the composite.

The reproducibility of thermal energy storage and release of composite S5 was verified by conducting repeated heating and cooling cycles. The temperature and heat flux evolutions are presented in Fig. 8.

3.6. Photothermal conversion performance

To determine the photothermal conversion behavior of the composites, cylindrical samples were heated under simulated solar irradiation for 30 min while recording the temperature and heat flux evolution.

Fig. 9 shows the temperature and heat flux-time evolution curves of composite S5. When the light irradiates, the temperature of the composite increases, confirming the photothermal conversion ability of the composite. The

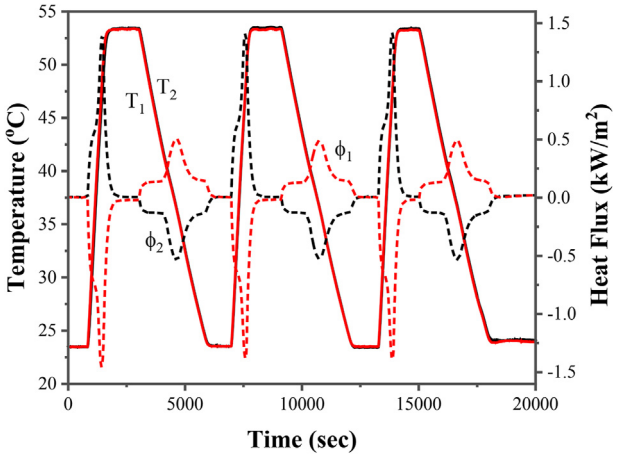

Fig. 8 – Heat flux and temperature evolution from solid to liquid for S5 for cyclic variation of temperature from 23 to 53 °C.

charging/discharging process consists of three stages, as shown in Fig. 9. The temperature and heat flux increase in the first stage indicates the solid sensible heat storage. In the second stage, the heat flux reaching the sample bottom decreases due to the start of latent heat storage. As the phase change progresses, the heat flux again increases rapidly. The temperature evolution curve shows a plateau at this stage. In the third stage, the rate of heat flux transferred to the sample bottom decreases at the end of the phase change. A rapid increase in temperature at this stage indicates the sensible heat storage of the liquid paraffin. During the discharge process, the order of the stage reverses, as shown in Fig. 9.

The difference between the top and bottom temperatures in the sensible heat region was constant. In the solid–liquid latent heat region, the difference between the top and bottom temperatures increases due to the energy storage as latent heat. During the discharge process, the temperature at the sample top was low due to the convective heat loss to the surrounding air through the sample top.

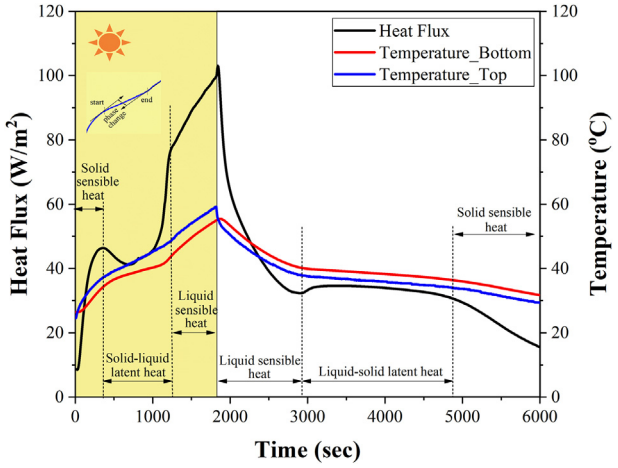

Fig. 9 – Temperature and heat flux evolution curves of S5 during photothermal conversion testing.

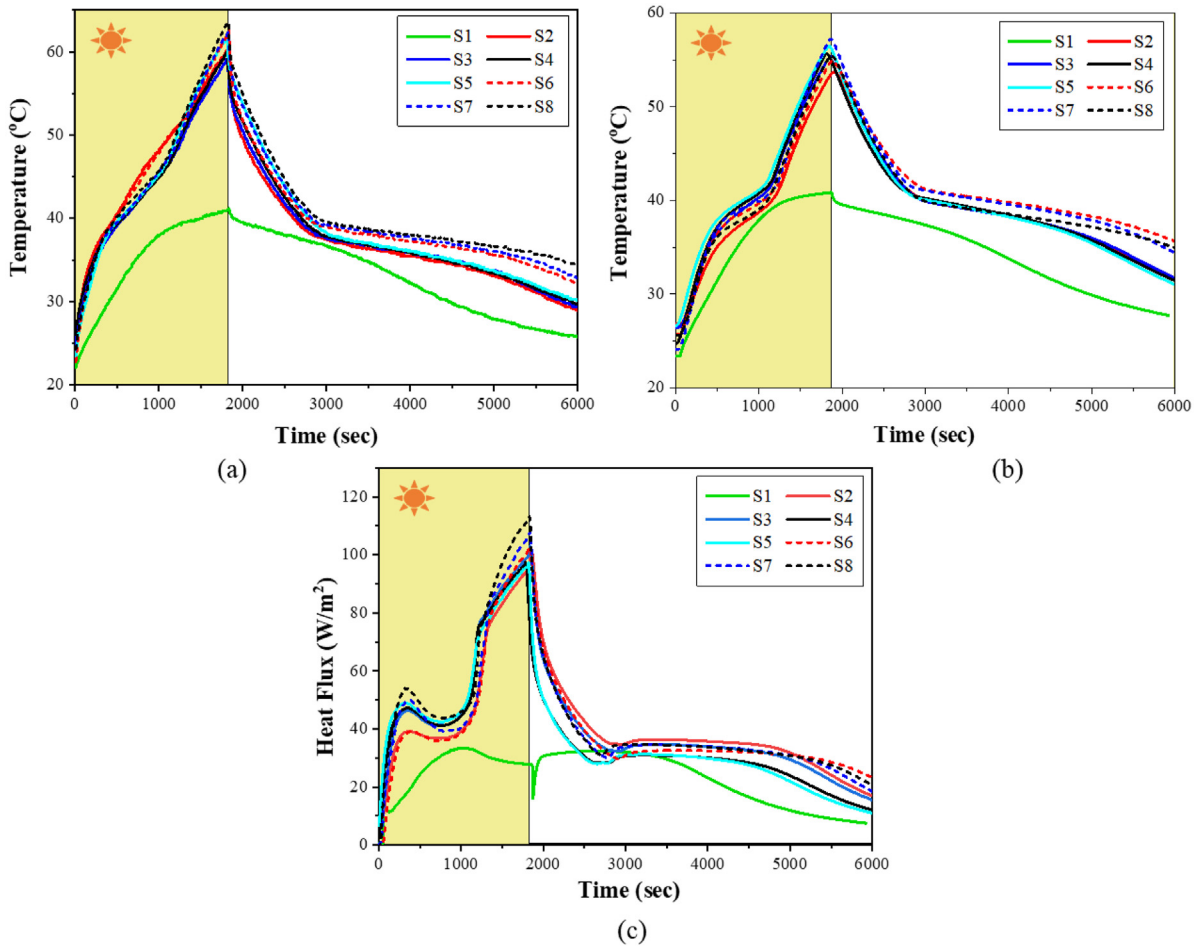

Fig. 10 – The evolution curves of different composites (S1–S8); (a) temperature at sample top surface, (b) temperature at sample bottom, and (c) heat flux passing through the samples.

Fig. 10 shows the temperature (sample top and bottom) and heat flux evolution curves of different composites.

The poor photoabsorption property of the composite without EG is clear in Fig. 10, as indicated by the lower temperature and heat flux values. As expected, the photoabsorption capacity of EG increased the sample top surface temperature with the increase in EG mass fraction (Fig. 10a). Moreover, the sample bottom temperature variation shows a clear trend of increasing temperature with increasing EG content (Fig. 10b). This can be explained by the rise in thermal conductivity of the composites with the increase in EG content. Fig. 10c shows the heat flux evolution curves of the composites.

The photothermal storage efficiency (η_p) was measured by the ratio of the latent heat of the paraffin (i.e., the total mass of paraffin in the composite (m) times its enthalpy (ΔH)) to the energy of simulated solar light during the phase change (i.e., the product of the power of applied light source (P), the exposed surface area of the sample (S) and time taken for phase change (Δt)). Therefore, the storage efficiency is

Table 5 – Photothermal energy storage performance of the composites considering latent heat only.

Sample	S1	S2	S3	S4	S5	S6	S7	S8
Mass (m, g)	26.82	28.49	30.51	31.30	32.08	29.06	31.51	31.24
Latent heat (ΔH, J/g)	62.0	42.6	44.7	40.9	47.7	60.8	62.4	64.1
Stored energy (J)	1663	1214	1363	1280	1530	1767	1966	2002
Phase change duration, Fig. 10a (Δt, s)	1800	750	790	710	795	780	750	690
Input energy (J)	6445	2650	2835	2545	2869	2780	2720	2510
Energy storage efficiency, (η_p, %)	25.8	45.8	48.1	50.3	53.3	63.6	72.3	79.8
Phase change duration, Fig. 10c (Δt, s)	1800	960	880	850	885	980	960	890
Input energy (J)	6445	3392	3158	3047	3193	3492	3482	3238
Energy storage efficiency (η_p, %)	23.0	35.8	43.2	42.0	47.9	50.6	56.5	61.8

Table 6 – Thermal properties of polymer phase change composites for photothermal conversion.

Polymeric PCM composite (polymer/PCM/filler)	PCM content (%)	Latent heat capacity (J/g)	Photothermal conversion efficiency (%)	Ref.
Melamine foam/PW/GNP	95	155.5	62.5	[56]
Melamine foam/PW/PDA	95	142.7	80.8	[57]
Gelatin aerogel/PW/$Ti_3C_2T_x$	97.7	199.9	–	[60]
Ethylene-Propylene-Diene Monomer/PW/EG	70	126.8	–	[39]
Thermoplastic elastomer/PW/EG	63	145.4	72	[37]
Polyethylene and ethylene-propylene rubber/PW/EG	70	138.7	70	[38]
Polyoxyethylene/PW/EG	70	126.7	58.2	[36]
Acrylamide-acrylic acid sodium copolymer/sodium acetate trihydrate/CuS	87	202.4	87.1	[58]
HDPE/PW/EG	50	64.1	79.8	This study

GNP- Graphene nanoplatelets, PDA- Polydopamine.

considering that all the paraffin in the composite participated in the phase change process.

$$\eta_p = \frac{m\Delta H}{PS\Delta t} \quad (5)$$

Fig. 10 (inset) shows the determination of the time taken for phase change based on previous studies [18,46,48,49,53–55]. However, the method is not reliable for two reasons: (1) the selection of wrong tangents would make a large difference in the calculated conversion efficiency, and (2) the method only considers the phase change of PCMs at the point of temperature measurement. However, as observed in Fig. 9, the temperature plateau started earlier at the sample top and ended later at the sample bottom. More interestingly, both are reflected in the heat flux curve, which would indicate the phase change process of the whole sample. On the other hand, the heat flux evolution curve helps to identify the regions of sensible and latent heat storage of the composite specimen during the photothermal conversion study. Therefore, in this study, the phase change duration was determined from the heat flux evolution curve (i.e., region for solid–liquid latent heat), as shown in Fig. 9. As observed in Fig. 10c, with the increase in EG content, the time taken for phase change decreases due to the increase in the thermal conductivity of the composite.

Table 5 shows the photothermal energy storage performance of the composites. For comparison, the energy storage efficiency calculated from the sample top temperature evolution curves (Fig. 10 a) and heat flux curve (Fig. 10 c) are given in the Table. As previously explained, the phase change duration was underestimated from the temperature evolution curve, as it does not consider the phase change in the whole sample. Therefore, the photothermal conversion efficiency is overestimated in previous studies [56–61]. As a result, the storage efficiency of sample S8 was 79.8%, while it was 61.8% when the phase change duration was taken from the heat flux curve. The composite was efficient in photothermal conversion, and the efficiency was much higher than that of previously reported polymer/paraffin phase change composites, even with a lower mass fraction of PCM and latent heat capacity, as given in Table 6. However, the actual photothermal conversion efficiency of the composite was 61.8%, which accounts for the phase change of all paraffins in the composite. Therefore, this study, for the first time in the literature, validates the assumption (in the photothermal conversion efficiency calculation) that all PCMs in the composite participated in the phase change process during the photothermal conversion study.

In addition to the latent heat, the composite stores the thermal energy as sensible heat. Considering the total energy storage density of the composite, the photothermal conversion efficiency can be calculated according to Eq. (6) [15,49,62]:

$$\eta_p = \frac{m\left(\int_{T_i}^{T_m} C_{ps}dT + \Delta H + \int_{T_m}^{T_f} C_{pl}dT\right)}{PSt} \quad (6)$$

where T_i and T_f are the initial and final sample temperatures before and after solar irradiation, T_m is the peak melting temperature of PW, C_{ps} and C_{pl} are the specific heat capacities of the composites in the solid and liquid states of PW estimated from TGHPT, and t is the total time of solar irradiation. Table 7 shows the conversion efficiencies of various composites considering the total energy storage density of the composite. The higher specific heat capacities of HDPE and PW contributed more than half of the total energy density as sensible heat during the photothermal conversion study.

Table 7 – Photothermal energy storage performance of the composites considering total energy storage density.

Sample	S1	S2	S3	S4	S5	S6	S7	S8
Sensible heat, solid (J/g)	54.7	48.9	46.6	46.8	42.3	45.0	44.0	46.8
Latent heat (ΔH, J/g)	62.0	42.6	44.7	40.9	47.7	60.8	62.4	64.1
Sensible heat, liquid (J/g)	–	27.0	30.3	27.1	30.0	26.5	27.3	27.6
Total energy storage density (J/g)	116.7	118.5	121.6	114.8	120.0	132.3	133.7	138.5
Input energy (J)	7217	6359	6460	6453	6495	6415	6528	6549
Stored energy (J)	3132	3376	3710	3594	3851	3844	4214	4327
Energy storage efficiency (η_p, %)	43.4	53.1	57.4	55.7	59.3	59.9	64.6	66.1

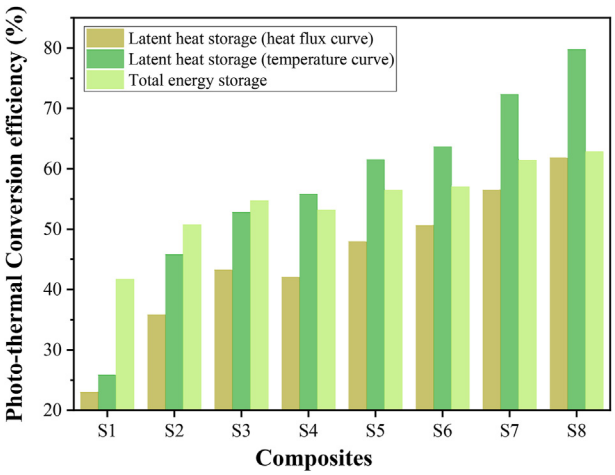

Fig. 11 – Photothermal conversion efficiency of the composites.

Fig. 11 shows the photothermal conversion efficiency of the composites estimated from the latent heat storage (from temperature and heat flux curves) and total energy storage. For the composite without EG, the efficiency calculated from the latent heat storage is very low for two reasons: (1) the poor photoabsorption capacity of the HDPE/PW composite and (2) the lower thermal conductivity.

It is evident from the plot that the presence of EG improved the photothermal conversion performance of the composite for two reasons. First, the higher photoabsorption capacity of EG increased the sample temperature from 41 °C to 57 °C. Second, the increased thermal conductivity of the composite with EG reduced the time required for phase change by fast heat transfer in the composite. Moreover, the larger mass fractions of PW (i.e., 50 wt%) in S6–S8 increased the conversion efficiency compared to the composites with 40 wt% PW.

The repeatability of the measurements was validated through 20 cycles of heating and cooling by solar exposure for composite S8, and the heat flux and temperature-time evolutions showed negligible variation, as shown in Fig. 12.

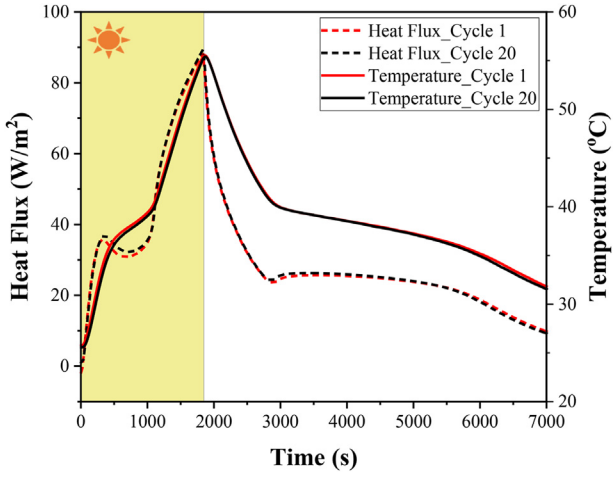

Fig. 12 – The heat flux and temperature evolution curves of S8 tested at 20 cycles of heating and cooling during the photothermal conversion study.

4. Conclusions

In this study, a shape-stabilized phase change composite was fabricated by the physical blending and hot pressing of HDPE, PW, and EG. The integration of EG into the composite significantly enhanced the thermal conductivity and reduced the PCM leakage of the composite. The composite with 20 wt% EG has a thermal conductivity of 0.81 W/m.°C, which was 305% higher than that of pure PW. The specific heat capacities and latent heat of the composites were investigated on macroscale specimens by homemade equipment based on the transient guarded hot plate technique. The latent heat of the composite varied in the range of 40.9–64.1 J/g. The photothermal conversion efficiency of the composite calculated from the temperature evolution curves increased from 25.8% to 79.8% with increasing EG and PW mass fractions. Since the efficiency calculated from the temperature curves is overestimated without accounting for the phase change of whole PCMs in the composite, heat flux curves were introduced in this paper for the first time. The sensible and latent heat regions identified in the heat flux evolution curve accurately estimated the phase change duration. Therefore, the actual conversion efficiency of S8 decreased from 79.8% (estimated from the conventional temperature curve) to 61.8%, which accounts for the complete phase change in the composite.

Moreover, considering the sensible heat storage capacity of the composite, S8 (i.e., HDPE/PW/EG: 35/50/15) exhibited a storage density of 138.5 J/g and a photothermal conversion and storage efficiency of 66.1%. The increase in EG and PW mass fraction increased the photothermal conversion efficiency due to the decreased phase change duration and increased latent heat, respectively. These photodriven composites provide new insight for effective utilization in solar energy conversion and storage applications.

Declaration of competing interest

The authors declare that they have no known competing financial interests or personal relationships that could have appeared to influence the work reported in this paper.

Acknowledgment

This work was made possible by the Award NPRP13S-0127–200177 from the Qatar National Research Fund (a member of The Qatar Foundation). SEM measurements of the samples were accomplished in the Central Laboratories Unit, at Qatar University. The statements made herein are solely the responsibility of the authors.

Appendix A. Supplementary data

Supplementary data to this article can be found online at https://doi.org/10.1016/j.jmrt.2023.04.047.

REFERENCES

[1] Kannan N, Vakeesan D. Solar energy for future world: - a review. Renew Sustain Energy Rev 2016;62:1092–105. https://doi.org/10.1016/J.RSER.2016.05.022.

[2] Shahsavari A, Akbari M. Potential of solar energy in developing countries for reducing energy-related emissions. Renew Sustain Energy Rev 2018;90:275–91. https://doi.org/10.1016/J.RSER.2018.03.065.

[3] Boldoo T, Ham J, Kim E, Cho H. Review of the photothermal energy conversion performance of nanofluids, their applications, and recent advances. Energies 2020;13:5748. https://doi.org/10.3390/EN13215748.

[4] Rawat R, Lamba R, Kaushik SC. Thermodynamic study of solar photovoltaic energy conversion: an overview. Renew Sustain Energy Rev 2017;71:630–8. https://doi.org/10.1016/J.RSER.2016.12.089.

[5] Tyagi Vv, Panwar NL, Rahim NA, Kothari R. Review on solar air heating system with and without thermal energy storage system. Renew Sustain Energy Rev 2012;16:2289–303. https://doi.org/10.1016/J.RSER.2011.12.005.

[6] Arunkumar HS, Vasudeva Karanth K, Kumar S. Review on the design modifications of a solar air heater for improvement in the thermal performance. Sustain Energy Technol Assessments 2020;39:100685. https://doi.org/10.1016/J.SETA.2020.100685.

[7] Vengadesan E, Senthil R. A review on recent development of thermal performance enhancement methods of flat plate solar water heater. Sol Energy 2020;206:935–61. https://doi.org/10.1016/J.SOLENER.2020.06.059.

[8] Zhang Y, Gurzadyan GG, Umair MM, Wang W, Lu R, Zhang S, et al. Ultrafast and efficient photothermal conversion for sunlight-driven thermal-electric system. Chem Eng J 2018;344:402–9. https://doi.org/10.1016/J.CEJ.2018.03.098.

[9] Wang P. Emerging investigator series: the rise of nano-enabled photothermal materials for water evaporation and clean water production by sunlight. Environ Sci Nano 2018;5:1078–89. https://doi.org/10.1039/C8EN00156A.

[10] Chaturvedi R, Islam A, Sharma K. A review on the applications of PCM in thermal storage of solar energy. Mater Today Proc 2021;43:293–7. https://doi.org/10.1016/J.MATPR.2020.11.665.

[11] Gulfam R, Zhang P, Meng Z. Advanced thermal systems driven by paraffin-based phase change materials – a review. Appl Energy 2019;238:582–611. https://doi.org/10.1016/J.APENERGY.2019.01.114.

[12] Karkri M, Lachheb M, Gossard D, ben Nasrallah S, Almaadeed MA. Improvement of thermal conductivity of paraffin by adding expanded graphite, 50; 2015. p. 2589–601. https://doi.org/10.1177/0021998315612535. Http://DxDoiOrg/101177/0021998315612535.

[13] Maithya OM, Zhu X, Li X, Korir SJ, Feng X, Sui X, et al. High-energy storage graphene oxide modified phase change microcapsules from regenerated chitin Pickering Emulsion for photothermal conversion. Sol Energy Mater Sol Cell 2021;222:110924. https://doi.org/10.1016/J.SOLMAT.2020.110924.

[14] Yuan K, Liu J, Fang X, Zhang Z. Crafting visible-light-absorbing dye-doped phase change microspheres for enhancing solar-thermal utilization performance. Sol Energy Mater Sol Cell 2020;218:110759. https://doi.org/10.1016/J.SOLMAT.2020.110759.

[15] Zhang Y, Li X, Li J, Ma C, Guo L, Meng X. Solar-driven phase change microencapsulation with efficient Ti4O7 nanoconverter for latent heat storage. Nano Energy 2018;53:579–86. https://doi.org/10.1016/J.NANOEN.2018.09.018.

[16] Umair MM, Zhang Y, Zhang S, Jin X, Tang B. A novel flexible phase change composite with electro-driven shape memory, energy conversion/storage and motion sensing properties. J Mater Chem A Mater 2019;7:26385–92.

[17] Maleki M, Karimian H, Shokouhimehr M, Ahmadi R, Valanezhad A, Beitollahi A. Development of graphitic domains in carbon foams for high efficient electro/photo-to-thermal energy conversion phase change composites. Chem Eng J 2019;362:469–81. https://doi.org/10.1016/J.CEJ.2019.01.032.

[18] Yang J, Tang L-S, Bao R-Y, Bai L, Liu Z-Y, Yang W, et al. An ice-templated assembly strategy to construct graphene oxide/boron nitride hybrid porous scaffolds in phase change materials with enhanced thermal conductivity and shape stability for light–thermal–electric energy conversion. J Mater Chem A Mater 2016;4:18841–51. https://doi.org/10.1039/C6TA08454K.

[19] Hu H. Recent advances of polymeric phase change composites for flexible electronics and thermal energy storage system. Compos B Eng 2020;195:108094. https://doi.org/10.1016/J.COMPOSITESB.2020.108094.

[20] Chriaa I, Karkri M, Trigui A, Jedidi I, Abdelmouleh M, Boudaya C. The performances of expanded graphite on the phase change materials composites for thermal energy storage. Polymer (Guildf) 2021;212:123128. https://doi.org/10.1016/J.POLYMER.2020.123128.

[21] Mochane MJ, Luyt AS. The effect of expanded graphite on the flammability and thermal conductivity properties of phase change material based on PP/wax blends. Polym Bull 2015;72:2263–83. https://doi.org/10.1007/S00289-015-1401-9/FIGURES/17.

[22] Sobolčiak P, Mrlik M, Popelka A, Minařík A, Ilcikova M, Srnec P, et al. Foamed phase change materials based on recycled polyethylene/paraffin wax blends. Polymers 2021;13:1987. https://doi.org/10.3390/POLYM13121987.

[23] Mochane MJ, Luyt AS. The effect of expanded graphite on the thermal stability, latent heat, and flammability properties of EVA/wax phase change blends. Polym Eng Sci 2015;55:1255–62. https://doi.org/10.1002/PEN.24063.

[24] Krupa I, Miková G, Luyt AS. Phase change materials based on low-density polyethylene/paraffin wax blends. Eur Polym J 2007;43:4695–705. https://doi.org/10.1016/J.EURPOLYMJ.2007.08.022.

[25] Cai Y, Hu Y, Song L, Kong Q, Yang R, Zhang Y, et al. Preparation and flammability of high density polyethylene/paraffin/organophilic montmorillonite hybrids as a form stable phase change material. Energy Convers Manag 2007;48:462–9. https://doi.org/10.1016/J.ENCONMAN.2006.06.021.

[26] Cai Y, Wei Q, Huang F, Gao W. Preparation and properties studies of halogen-free flame retardant form-stable phase change materials based on paraffin/high density polyethylene composites. Appl Energy 2008;85:765–75. https://doi.org/10.1016/J.APENERGY.2007.10.017.

[27] Cai Y, Wei Q, Huang F, Lin S, Chen F, Gao W. Thermal stability, latent heat and flame retardant properties of the thermal energy storage phase change materials based on paraffin/high density polyethylene composites. Renew Energy 2009;34:2117–23. https://doi.org/10.1016/J.RENENE.2009.01.017.

[28] Sobolciak P, Karkri M, Al-Maadeed MA, Krupa I. Thermal characterization of phase change materials based on linear low-density polyethylene, paraffin wax and expanded graphite. Renew Energy 2016;88:372–82. https://doi.org/10.1016/J.RENENE.2015.11.056.

[29] Cheng G, Wang X, He Y. 3D graphene paraffin composites based on sponge skeleton for photo thermal conversion and

energy storage. Appl Therm Eng 2020;178:115560. https://doi.org/10.1016/J.APPLTHERMALENG.2020.115560.
[30] Li M, Wang C. AAZO-Graphene composite phase change materials with Photo-thermal conversion performance. Sol Energy 2021;223:11–8. https://doi.org/10.1016/J.SOLENER.2021.05.036.
[31] Zhang Q, Zhang Z, Xia W, Zhou Y, Yang H. Enhanced thermal conductive lauric acid/g-C3N4/graphene composite phase change materials for efficient photo-thermal storage. Fuel 2023;333:126279. https://doi.org/10.1016/J.FUEL.2022.126279.
[32] Chen Y, Zhang Q, Wen X, Yin H, Liu J. A novel CNT encapsulated phase change material with enhanced thermal conductivity and photo-thermal conversion performance. Sol Energy Mater Sol Cell 2018;184:82–90. https://doi.org/10.1016/J.SOLMAT.2018.04.034.
[33] Sun Q, Zhang N, Zhang H, Yu X, Ding Y, Yuan Y. Functional phase change composites with highly efficient electrical to thermal energy conversion. Renew Energy 2020;145:2629–36. https://doi.org/10.1016/J.RENENE.2019.08.007.
[34] Cao Y, Fan D, Lin S, Ng FTT, Pan Q. Branched alkylated polynorbornene and 3D flower-like MoS2 nanospheres reinforced phase change composites with high thermal energy storage capacity and photothermal conversion efficiency. Renew Energy 2021;179:687–95. https://doi.org/10.1016/J.RENENE.2021.07.028.
[35] Yang M, Dong H, Sun K, Kou Y, Zhang L, Zhao J, et al. Scalable synthesis of paraffin@MoS2-melamine foam composite phase change materials with superior photo-thermal conversion and storage. J Energy Storage 2022;56:105954. https://doi.org/10.1016/J.EST.2022.105954.
[36] Zou X, Liu J. Polyoxyethylene based phase change materials with enhanced mechanical property, thermal conductivity and photo-thermal energy charging capacity. Energy Rep 2020;6:2948–55. https://doi.org/10.1016/J.EGYR.2020.10.022.
[37] Cai Z, Liu J, Zhou Y, Dai L, Wang H, Liao C, et al. Flexible phase change materials with enhanced tensile strength, thermal conductivity and photo-thermal performance. Sol Energy Mater Sol Cell 2021;219:110728. https://doi.org/10.1016/J.SOLMAT.2020.110728.
[38] Chen Y, Gao S, Liu C, Situ Y, Liu J, Huang H. Preparation of PE-EPDM based phase change materials with great mechanical property, thermal conductivity and photo-thermal performance. Sol Energy Mater Sol Cell 2019;200:109988. https://doi.org/10.1016/J.SOLMAT.2019.109988.
[39] Liu J, Zou X, Cai Z, Peng Z, Xu Y. Polymer based phase change material for photo-thermal utilization. Sol Energy Mater Sol Cell 2021;220:110852. https://doi.org/10.1016/J.SOLMAT.2020.110852.
[40] Castellón C, Günther E, Mehling H, Hiebler S, Cabeza LF. Determination of the enthalpy of PCM as a function of temperature using a heat-flux DSC - a study of different measurement procedures and their accuracy. Int J Energy Res 2008;32:1258–65. https://doi.org/10.1002/ER.1443.
[41] Li C, Yu H, Song Y, Liu Z. Novel hybrid microencapsulated phase change materials incorporated wallboard for year-long year energy storage in buildings. Energy Convers Manag 2019;183:791–802. https://doi.org/10.1016/J.ENCONMAN.2019.01.036.
[42] Trigui A, Karkri M, Boudaya C, Candau Y, Ibos L, Fois M. Http://DxDoiOrg/101177/0021998312468185. Experimental investigation of a composite phase change material: thermal-energy storage and release, 48; 2012. p. 49–62. https://doi.org/10.1177/0021998312468185.
[43] Trigui A, Karkri M, Boudaya C, Candau Y, Ibos L. Development and characterization of composite phase change material: thermal conductivity and latent heat thermal energy storage. Compos B Eng 2013;49:22–35. https://doi.org/10.1016/J.COMPOSITESB.2013.01.007.
[44] Moulahi C, Trigui A, Boudaya C, Karkri M. Http://DxDoiOrg/101177/0892705715614065. Smart macroencapsulated resin/wax composite for energy conservation in the built environment: thermophysical and numerical investigations, 30; 2015. p. 887–914. https://doi.org/10.1177/0892705715614065.
[45] Trigui A, Karkri M, Krupa I. Thermal conductivity and latent heat thermal energy storage properties of LDPE/wax as a shape-stabilized composite phase change material. Energy Convers Manag 2014;77:586–96. https://doi.org/10.1016/J.ENCONMAN.2013.09.034.
[46] Yang L, Yuan Y, Zhang N, Dong Y, Sun Y, Ji W. Photo-to-thermal conversion and energy storage of lauric acid/expanded graphite composite phase change materials. Int J Energy Res 2020;44:8555–66. https://doi.org/10.1002/ER.5542.
[47] Li T, Wu M, Wu S, Xiang S, Xu J, Chao J, et al. Highly conductive phase change composites enabled by vertically-aligned reticulated graphite nanoplatelets for high-temperature solar photo/electro-thermal energy conversion, harvesting and storage. Nano Energy 2021;89:106338. https://doi.org/10.1016/J.NANOEN.2021.106338.
[48] Li M, Wang C. Preparation and characterization of GO/PEG photo-thermal conversion form-stable composite phase change materials. Renew Energy 2019;141:1005–12. https://doi.org/10.1016/J.RENENE.2019.03.141.
[49] Wang H, Ci E, Li X, Li J. The magnesium nitrate hexahydrate with Ti4O7 composite phase change material for photo-thermal conversion and storage. Sol Energy 2021;230:462–9. https://doi.org/10.1016/J.SOLENER.2021.10.063.
[50] Standard Test Method for Steady-State Thermal Transmission Properties by Means of the Heat Flow Meter Apparatus n.d. https://www.astm.org/standards/c518 (accessed April 24, 2022).
[51] Standard Test Method for Using a Heat Flow Meter Apparatus for Measuring Thermal Storage Properties of Phase Change Materials and Products n.d. https://www.astm.org/c1784-20.html (accessed October 10, 2022)..
[52] Cao R, Liu H, Chen S, Pei D, Miao J, Zhang X. Fabrication and properties of graphene oxide-grafted-poly(hexadecyl acrylate) as a solid-solid phase change material. Compos Sci Technol 2017;149:262–8. https://doi.org/10.1016/J.COMPSCITECH.2017.06.019.
[53] Aftab W, Mahmood A, Guo W, Yousaf M, Tabassum H, Huang X, et al. Polyurethane-based flexible and conductive phase change composites for energy conversion and storage. Energy Storage Mater 2019;20:401–9. https://doi.org/10.1016/J.ENSM.2018.10.014.
[54] Hu L, Li X, Ding L, Chen L, Zhu X, Mao Z, et al. Flexible textiles with polypyrrole deposited phase change microcapsules for efficient photothermal energy conversion and storage. Sol Energy Mater Sol Cell 2021;224:110985. https://doi.org/10.1016/J.SOLMAT.2021.110985.
[55] Li B, Nie S, Hao Y, Liu T, Zhu J, Yan S. Stearic-acid/carbon-nanotube composites with tailored shape-stabilized phase transitions and light–heat conversion for thermal energy storage. Energy Convers Manag 2015;98:314–21. https://doi.org/10.1016/J.ENCONMAN.2015.04.002.
[56] Xue F, Lu Y, dong Qi X, hui Yang J, Wang Y. Melamine foam-templated graphene nanoplatelet framework toward phase change materials with multiple energy conversion abilities. Chem Eng J 2019;365:20–9. https://doi.org/10.1016/J.CEJ.2019.02.023.
[57] Wu HY, Chen RT, Shao YW, Qi XD, Yang JH, Wang Y. Novel flexible phase change materials with mussel-inspired modification of melamine foam for simultaneous light-actuated shape memory and light-to-thermal energy storage capability. ACS Sustain Chem Eng 2019;7:13532–42. https://

doi.org/10.1021/ACSSUSCHEMENG.9B03169/ASSET/IMAGES/LARGE/SC-2019-03169R_0009.JPEG.

[58] Xiao Q, Fan J, Li L, Xu T, Yuan W. Solar thermal energy storage based on sodium acetate trihydrate phase change hydrogels with excellent light-to-thermal conversion performance. Energy 2018;165:1240–7. https://doi.org/10.1016/J.ENERGY.2018.10.105.

[59] Du X, Qiu J, Deng S, Du Z, Cheng X, Wang H. Ti3C2Tx@PDA-Integrated polyurethane phase change composites with superior solar-thermal conversion efficiency and improved thermal conductivity. ACS Sustain Chem Eng 2020;8:5799–806. https://doi.org/10.1021/ACSSUSCHEMENG.0C01582/ASSET/IMAGES/LARGE/SC0C01582_0009.JPEG.

[60] Liu X, Lin F, Zhang X, Liu M, Sun Z, Zhang L, et al. Paraffin/Ti3C2T xMxene@Gelatin aerogels composite phase-change materials with high solar-thermal conversion efficiency and enhanced thermal conductivity for thermal energy storage. Energy Fuel 2021;35:2805–14. https://doi.org/10.1021/ACS.ENERGYFUELS.0C04275/SUPPL_FILE/EF0C04275_SI_001.PDF.

[61] Mo Z, Mo P, Yi M, Hu Z, Tan G, Selim MS, et al. Ti3C2Tx@Polyvinyl alcohol foam-supported phase change materials with simultaneous enhanced thermal conductivity and solar-thermal conversion performance. Sol Energy Mater Sol Cell 2021;219:110813. https://doi.org/10.1016/J.SOLMAT.2020.110813.

[62] Wang T, Wang K, Ye F, Ren Y, Xu C. Characterization and thermal properties of a shape-stable Na2CO3-K2CO3/coal fly ash/expanded graphite composite phase change materials for high-temperature thermal energy storage. J Energy Storage 2021;33:102123. https://doi.org/10.1016/J.EST.2020.102123.